# PCCP

# Characterization of amorphous Li$_x$Si structures from ReaxFF via accelerated exploration of local minima[†]

Francisco Fernandez,[a,b] Sergio Alexis Paz,[c,d] Manuel Otero,[a,b] Daniel Barraco,[a,b] and Ezequiel P. M. Leiva,[*c,d]

Motivated by the abundant experimental work in the area of Li-ion batteries, in the present work we characterize via computer simulations the structure of Si-Li amorphous alloys in a wide range of compositions. Using a reactive force field we propose a novel accelerated exploration of local minima to obtain amorphous structures close to equilibrium. The features of this system analyzed for different alloy compositions are the partial radial distribution functions g(r), the first and second nearest neighbour coordination numbers and the short-order structure. The complex structure of the second peak of the Si-Li g(r) is elucidated by a cluster-connection analysis.

## 1 Introduction

Lithium ion batteries (LIBs) are devices that transform available electrical energy into chemical energy that can be transformed back and used as electrical energy as is needed, for example, in electric vehicles. The usual anode for LIBs is based on graphite, having a theoretical capacity of 372 mAhg$^{-1}$, several approaches has been developed to boost this capacity in carbon based anodes[1,2]. On the other hand, at the beginning of this century, silicon has been proposed as an anode material to replace graphite due to its abundance, low cost, low discharge voltage and high theoretical capacity of 3579 mAhg$^{-1}$. However, this material exhibits a large volume expansion, of about 300% at full lithiation and structural changes that lead to capacity degradation and short cycle life[3]. In this electrochemical cycling, Li reacts with Si to form amorphous Li$_x$Si alloys. Hence the importance of studying the amorphous phases rather than the crystalline ones for the case of lithiated Si electrodes[4].

The experimental information about the structure of the different phases formed during the cycling of the Li$_x$Si electrode is very limited. Bulk and interfacial structures are unstable and amorphous structures are difficult to characterize by traditional experimental techniques. X-ray diffraction allowed to characterize a crystalline Li$_{15}$Si$_4$ phase in the electrode at full lithiation[5],

but this technique has shortcomings to study all the amorphous structures that form during the process of charge and discharge. Additionally, ex-situ Si pair distribution function (PDF) analysis of X-ray data made it possible to investigate the short-range order in amorphous Li$_x$Si structures[6] and to propose a lithiation mechanism. However, since X-ray has low sensitivity for light elements like Li, the conclusions are mainly based on the formation of small Si clusters and isolated Si during lithiation and limited for describing the structure at a larger scale. In this scenario, computer simulations stand like a powerful tool to get inside into the Li$_x$Si structures and its changes during lithiation. Although a unique and robust computational model to study all the different stages of the silicon electrode does not exist yet, several efforts has been made in the last years towards this direction.

The main obstacles that must be overcome in the computer simulation of silicon electrodes are related to the intrinsic multiscale nature of the system. Despite their great precision, DFT studies are drastically limited in the number of atoms that can be used to model the complex structures of lithium-silicon phases. Semi-empirical potentials appear as a solution to this issue, but robust and transferable parametrizations are required. Fan *et al.*[7] have parametrized a force field for Li-Si systems using the ReaxFF developed by Van Duin *et al.*[8]. They have optimized this force field using DFT calculations, considering data of energies, geometries and charges of crystal phases of Li, Si and different crystalline Li-Si alloys. In their work, Molecular Dynamics (MD) simulations were used to characterize mechanical properties of amorphous Li$_x$Si, including yield and fracture strengths, thin-film lithiation, biaxial compression, uniaxial tension and compression[7].

Fan *et al.* force field has been widely used with MD to study the lithiation process of different silicon structures, from bulk phases to nanostructures. Structure, stress, and diffusivity has been

$^a$ *Universidad Nacional de Córdoba. Facultad de Matemática, Astronomía, Física y Computación. Córdoba (X5000HUA), Argentina.*

$^b$ *Consejo Nacional de Investigaciones Científicas y Técnicas (CONICET), Instituto de Física Enrique Gaviola, Córdoba (X5000HUA), Argentina.*

$^c$ *Universidad Nacional de Córdoba. Facultad de Ciencias Químicas. Departamento de Química Teórica y Computacional. Córdoba (X5000HUA), Argentina.*

$^d$ *Consejo Nacional de Investigaciones Científicas y Técnicas (CONICET), Instituto de Fisicoquímica de Córdoba (INFIQC), Córdoba (X5000HUA), Argentina.*

studied during lithiation of amorphous silicon (a-Si) and crystals (c-Si) with different crystallographic orientations[9,10]. Ding *et al.*[11] have reported the variation of the migration velocity of phase boundary and diffusivity of Li as a function of external stress, pointing out that tensile stress accelerates the lithiation rate, while the compressive stress retards it. Kim *et al.*[12] performed MD simulations to characterize the structural evolution of the phase boundary between c-Si at different orientation planes with amorphous $Li_{15}Si_4$. Nanostructures have been studied also by Fan *et al.*[13], who computed the mechanical response of (111)-oriented c-Si nanopillar during lithiation. Similar work has been carried out for the (100)-oriented c-Si nanopillar by Cao *et al.*[14]. Tang *et al.*[15] investigated the evolution and survivability of porosity in Si nanosheets during the lithiation and delithiation processes. Ostadhossein *et al.*[16] characterize the lithiation in c-Si nanowires and showed that it can accurately reproduce the energy barriers of Li migration from DFT in both c-Si and a-Si. ReaxFF had been also used with other simulations methods. Grand Canonical Monte Carlo simulations were used to study one cycle of lithiation and delithiation of a-Si electrode[17]. Trochet and Mousseau[18] have characterized the energy landscape at relatively low concentrations of Li impurities in c-Si, using the kinetic activation-relaxation technique. Kim *et al.*[19] have developed an algorithm to investigate the delithiation responses of an aluminum-oxide coated silicon thin-film. ReaxFFs have been also combined with other force fields, like Tersoff and Lennard Jones potentials, to simulate the lithiation of coated-carbon Si nanoparticles, observing a correlation between the growth of stress and charge density[20,21]. Mechanical properties of lithiated $Si/SiO_2$ interface have been also reported by Verners and Simone[22]. We acknowledge the fact that the use of a ReaxFF does not allow the study of electronic properties. However, we can see from the previous discussion that it has been able to predict an important number of properties for the Li/Si system, and as we will see below, this is also the case of Li-Si amorphous alloys.

While MD simulations are a powerful predictive method to study the lithiation process, the time scale of these simulations are limited to only a few ns or $\mu$s. The number of operations required by a computer to reach the time scale of the operation of an experimental battery is prohibitive, even considering the use of semi-empirical potential like ReaxFF on large supercomputers. As a consequence the phase-space exploration is not enough and the lithium-silicon structures observed will be limited to those near the initial configuration, despite other configurations probably occur in the real-life system. Addressing the short time scale problem is the main issue in computer simulations and several approaches have been proposed[23–39]. However, the implementation and set-up of accelerated simulation methods is not straightforward, especially in the study of complex condensed systems[40–43]. For instance, free-energy based methods for enhancing exploration requires the definition of collective variables that capture the low-frequency degrees of the system[23–28]. Such definition is difficult to make when there is no prior knowledge to where direct the phase-space exploration. A simple but powerful method to accelerate the exploration of local minima in the molecular system is the simulated annealing[44]. The basic idea

is to enhance the phase-space exploration of MD or Monte Carlo simulations using high temperatures, and then progressively reduce the temperature to find an energy minimum. Multiple simulated annealing (MSA) have been previously used to explore and find several relevant minima structures close to equilibrium[45].

In the present work, we characterize the structure of Li-Si amorphous alloys in a wide range of compositions as described by the aforementioned ReaxFF. We use an accelerated exploration of local minima, which is similar to MSA but instead of heating and slowly cooling the system, we use an energy bias function to overcome the energetic barriers followed by local minimization to find the minima. This method allows us to obtain many energy minima structures, which are of interest to understand the structure of heavily cycled Si-Li electrodes. To the best of our knowledge, this is the first time that such an approach is taken for the study of this system.

## 2 Methods

In this work, we studied the properties of amorphous structures of $Li_xSi$ for different values of $x$ ranging from 0.21 to 4.2. Crystalline LiSi structures were obtained from the Materials Project[46] as initial states (see Supporting Information). To get initial structures with a desired $x$, the crystalline structure that has an immediately higher value of $x$ was selected. Then, a Li atom was removed at random and an NPT dynamic was carried out during 2.0 ps. For this simulation, a Nosé-Hoover thermostat[47,48] at 300.0 K and a barostat at 0.0 atm with a timestep of 1.0 fs was set using LAMMPS[49]. The removal of a Li atom at random and the NPT simulation were repeated until the desired concentration $x$ was reached. Finally, the frame with the lowest absolute pressure was selected as the initial state for the accelerated exploration of local minima, as described in the next section. The accelerated simulations were carried out in an NVT ensemble at 300.0 K with a Langevin thermostat using a modified version of GEMS[50]. In all cases, the size of the system is around thousands of atoms.

### 2.1 Accelerated exploration of local minima (AELM)

Li-Si alloys present strong interactions between the constituting atoms. This is particularly clear in the case of the Si-Si bond, where the bond energy is of the order of 2 eV[51]. Potential energy barriers are expected to be of this order of magnitude so that a molecular dynamics sampling of the room temperature properties in the present system appears hopeless. To widely explore the different configurations of the system, $\vec{r}$, we transformed the potential energy surface (PES), $V(\vec{r})$, by using:

$$V_b(\vec{r}) = V(\vec{r}) + (\alpha - 1)V(\vec{r}) = \alpha V(\vec{r}) \qquad (1)$$

where $\alpha$ is the compression factor. Equation 1 leads to a reduction of the barriers of the PES, so that the residence time in metastable states is shorter and the exploration of the different system configuration is more efficient and is reached in a reasonable simulation time. The term $(\alpha - 1)V(\vec{r})$ is usually known as "bias function".

The addition of a bias function to the PES is the basis of the hyperdynamics method (HD) developed by Voter[52,53]. This method was developed to accelerate the exploration of a system with-

out loosing its dynamics. In a typical HD simulation, to recover the average of some property, the sampled configuration are reweighted by a $w$ factor that involves an exponential function and depends on the applied bias. As stated above, the systems studied in this work involve large changes in the interaction energies, as compared with the thermal energy $kT$. In this way, the exponential function involved in the $w$s takes very large values, the procedure becomes numerically unstable and the recovery of properties like the average potential energy is not straightforward. Since we are not interested in the recovery of the real time elapsed during the simulation, the use of HD in this work is meant to perform an extensive exploration of the potential energy surface. Furthermore, since we are here interested in the structural properties at relatively low (room) temperatures, it is expected that once local minima are reached, the system will explore configurations close to them. Thus, we apply the conjugate gradient method (CG) to each frame of the HD and in this way we can sample the multiplicity of local structures that result from the present potential energy.

Our exploration method resembles simulated annealing, although our goal is to explore many different structures rather than finding the global minimum. Simulating annealing has been previously used for that purpose. For instance, Hao *et al.* used multiple simulated annealing simulation to obtain several minimum structures of peptides[45]. To continue with the analogy, in our accelerated exploration of local minima (AELM) we use HD instead of high temperatures to enhance the exploration, and multiple CG minimizations instead of simulated cooling to find the structures of the local minima. Figure S1 of supplementary information shows the histograms of the minimum energy obtained using the CG method after HD simulations with different $\alpha$s for different alloy compositions. From these plots, we selected the most suited acceleration factor leading to the minimum energy values from which we got the structural properties of the present alloys. Information about the size of the system and the number of structures used to obtain the following results can be consulted in Table 1 of the Supporting Information.

## 3 Results and discussion

Figure 1 shows the fractional volume changes with respect to pure c-Si of the initial states generated for the Li$_x$Si structures. Each point was calculated by a normalization relative to the number of atoms of Si in the structure according to:

$$fvc = \frac{N_{Si}}{V_{Si}} \left( \frac{V_{Si,x}}{N_{Si,x}} - \frac{V_{Si}}{N_{Si}} \right), \qquad (2)$$

where $V_{Si}$ and $N_{Si}$ are the volume and the number of atoms in the unit cell of c-Si, $V_{Si,x}$ and $N_{Si,x}$ are the volume and the number of Si atoms in the simulation cell for the corresponding $x$ value. Comparison with experimental data using atomic force microscopy (AFM) measured by Beaulieu *et al.*[54] and with the prediction of density functional calculations (DFT) with a fixed volume protocol used by Chevrier and Dahn[55] shows that the present ReaxFF delivers the correct qualitative and quantitative trends.

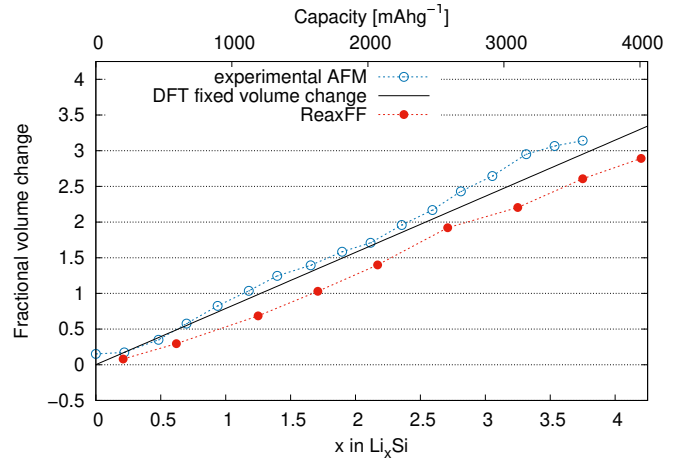Figure 2 shows histograms for the minimum energies of the Li$_x$Si structures obtained with AELM for different values of $x$ and



**Fig. 1** Fractional volume change as a function of alloy composition. Experimental values using AFM are shown in blue dots[54], full line are DFT calculations from refrence[55] and red dots are results of this work.

the compression factor $\alpha$. In the first case, where $x = 0.21$, we can appreciate how the use of smaller values of $\alpha$ allows finding structures with lower energies. The main effect of the $\alpha$ value on the PES is the compression of its energy barriers, allowing to enhance the phase-space exploration. This effect becomes more drastic as $\alpha$ value tends to zero. In the figure we can see that ordinary MD simulations ($\alpha = 1$) are not able to overcome the energy barriers during the simulated time, remaining the system close to the local minimum associated with the initial configuration. On the contrary, the use of $\alpha = 0.2$ in the AELM framework results in the rapid access to lower energies structures. A similar behaviour can be seen in Figure 2 for $x = 2.17$. However, in this case the small value of $\alpha = 0.2$ tends to yield higher energies than the other cases, yielding a distribution similar to that of ordinary MD but with greater fluctuations. This is probably due to an overly extended exploration, where the system diffuses trough a large region of the phase space and the multiple minimizations with CG are not able to find lower minima. Finally, for the last case shown in the figure, $x = 4.2$, the AELM simulation with $\alpha = 0.2$ is able to find structures that strongly reduce the potential energy of the system. Minimum energy histograms for $x = 0.21$, 2.17 and 4.2 are representative of the histograms obtained at different x, as can be seen in the Figure S1 of the Supporting Information.

In Figure 2 we have also included representative structures obtained from the AELM simulations of the Li$_x$Si systems with the different $x$ values studied and using the $\alpha$ parameters that give the lowest energy distribution for each case. For $x = 0.21$, it can be seen that the amorphous network of silicon remains with its tetrahedral structure distorted. Some of the Si-Si bonds start to break as the concentration of lithium increases, as can be seen for the $x = 2.17$ structure. Finally, for higher concentrations of lithium, like $x = 4.2$, some remarkable structures involving 1-periodic chains are reached. A similar structure has been previously reported by Ostadhossein *et al.*[16]. We will further characterize the different structures in the next sections of this work.

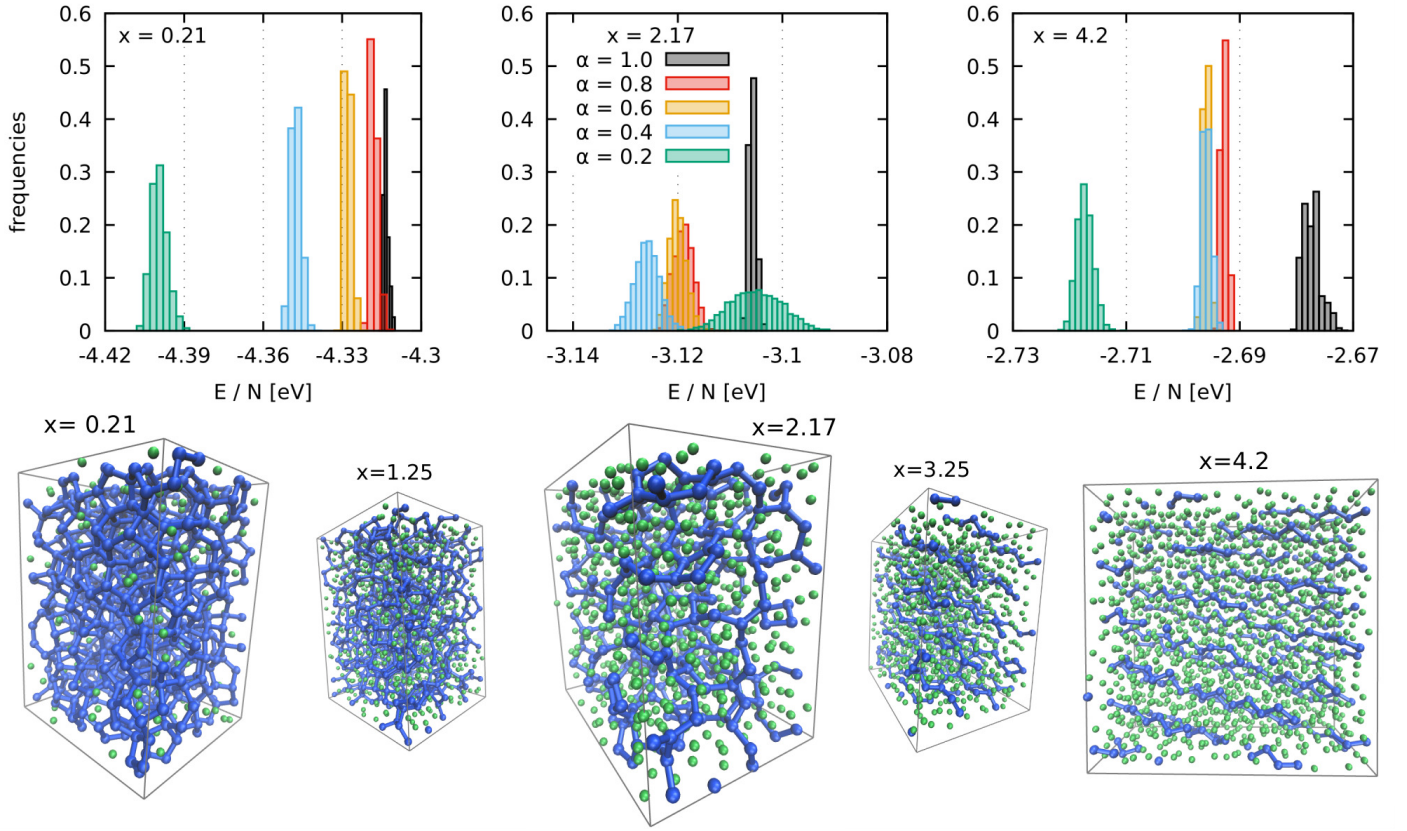The previous energy calculations can be used to test the per-

**Fig. 2** Histograms corresponding to the potential energy of the structures obtained trough the hyperdynamics with different $\alpha$s in equation 1, after minimization with conjugated gradients. The composition of the alloy is given by the $x$ value included in the figure and representative configurations are shown at the bottom of the figure. Silicon atoms are in blue and lithium atoms in green.

formance of the model to predict electrochemical properties, as suggested by Chevrier and Dahn[55]. First, we define the formation energy of the different amorphous alloys as

$$E_f(x) = E_{Li_xSi} - (xE_{Li} + E_{Si}), \qquad (3)$$

where $E_{Li_xSi}$ is the energy of the alloy per Si atom, and $E_{Li}$ and $E_{Si}$ are the cohesive energies of the Li and Si bulk materials. Using the previous formation energies as an approximation to the Gibbs formation energy, the potential versus Li metal of $Li_xSi$ can be obtained from

$$V(x) = -\frac{dE_f(x)}{dx}, \qquad (4)$$

where $V$ is the potential. Thus, the previous equation may be used to compare with previous experimental and theoretical results. The formation energies calculated according to equation 3 are given in Table 2 of Supplementary Information. From a spline of these values, shown in the inset of Figure 3, $V(x)$ values were obtained using equation 4 and are plotted as a function of composition in Figure 3 as a red line. For comparison, we include in the same figure the experimental curve obtained from lithiation and delithiation of sputtered amorphous silicon[56] and the theoretical curve from first-principles calculations[55]. It can be stated that the ReaxFF results are quite satisfactory.

## 3.1 Radial distribution functions

The pair radial distribution function (RDF), $g(r)$, characterizes the local structure of a fluid, and describes the probability to find an atom in a shell at a distance $r$ from a reference atom. In this work, this quantity is calculated as the ratio between the average density $\rho$ at distance $r$ from the reference atom and the density at that same distance of an ideal gas. In the case of multiple component systems, as in the present case, partial radial distribution functions can be calculated[57]. Figure 4 shows the results obtained for the RDF of Li-Li, Si-Li and Si-Si. Each one of them has a plot for each value of $x$ studied and the curves are calculated over the minimized frames of the HD.

The first peak of $RDF_{Li-Li}$ starts centered at 2.45 Å for the lowest concentration of Li ions and then its position increases with $x$ and remains around 2.95 Å for $x$ higher than 1.71. The peak height increases 50% after complete lithiation, relative to the lowest concentration. Regarding the first peak of the $RDF_{Si-Si}$, we observe that its center is located 2.4 Å for $x = 0.21$ and then it is shifted to higher distances. Beyond $x = 1.25$ the center is between 2.52 and 2.56 Å. The width of the peak decreases, the value of the FWHM goes from 0.14 Å for $x = 0.21$ to 0.05 Å for $x = 3.75$. As this happens, the height of the peak increases. On the other hand, the second peak of $RDF_{Si-Si}$ also shifts its center to higher distances, it splits into two peaks for $x$ between 0.62 and 1.71, and it appears again as a single peak for larger $x$. Between the first and the sec-
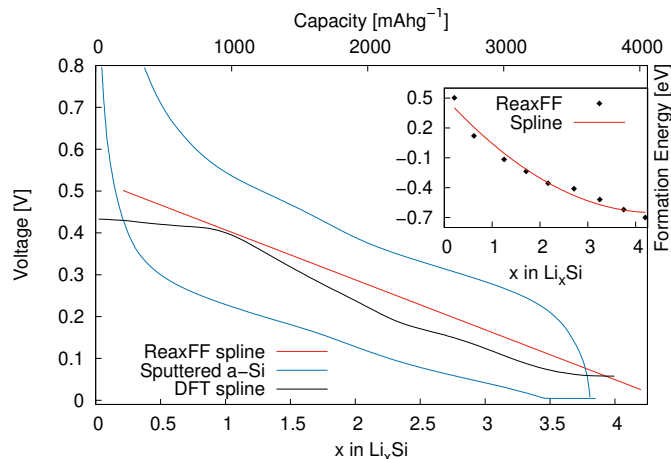
**Fig. 3** Potential-composition curves of the lithiation of Si anodes. The black line corresponds with DFT calculations from reference [55], the blue line corresponds with the experimental curve obtained from the lithiation of sputtered a-Si [56] and the red line is the derivative of the spline adjusted to the ReaxFF data of formation energy showed as an inset.

ond peak, a shoulder can be observed, as noted previously by Fan *et al.* [7]. The obtained results for the $RDF_{Si-Si}$ are in concordance with the experimental ones reported by Key *et al.* [6].

For the $RDF_{Si-Li}$, we find that the center of the first peak shifts to lower distances as the concentration of Li increases. Along with this shift, the width of the peak is reduced and its height is increased. We see that the second peaks of $RDF_{Si-Li}$ also shifts its center to lower distances, but above $x = 1.71$, the peak splits into two peaks with different heights depending on the $x$ value. To determine what causes this splitting in the $RDF_{Si-Li}$, an analysis similar to the one reported by Ding *et al.* [58] was performed. These authors analyzed the second-nearest-neighbour pair correlation distance in terms of cluster connections, defining a coordination polyhedra around the central atom considered for the RDF and its second neighbours. The number of shared atoms between these two linked coordination polyhedra were used to establish categories and analyze their contributions to the RDF. These categories depended on the fact that these polyhedra were sharing a vertex (1 atom), an edge (2 atoms), a face of polyhedra (3 atoms) or distorted quadrilateral or squashed tetrahedra (4 atoms). In a similar way to the aforementioned work, we deconvoluted the second peak of the RDF by calculating the partial RDF of each category. That is, each category is defined by the number of Li atoms interconnecting a Si atom with its second Li neighbours. The evolution of the $RDF_{Si-Li}$ behaviour is detailed in the Supporting Information. While the behaviour is rather complex as can be observed in Figure S2, it can be stated as a general trend that the higher component of $RDF_{Si-Li}$ , which is between 5.0 Å and 5.6 Å, corresponds to the atoms that have one, two or no Li connections. On the other hand, the 2nd nearest neighbour contribution to $RDF_{Si-Li}$, between 4.0 Å and 5.0 Å can be attributed to those atoms that have two or more Li interconnections. Thus, it can be broadly stated that at low concentrations of Li in the alloys, there is a predominance of second neighbour Li atoms that have one or no interconnection with Li neighbours of the first
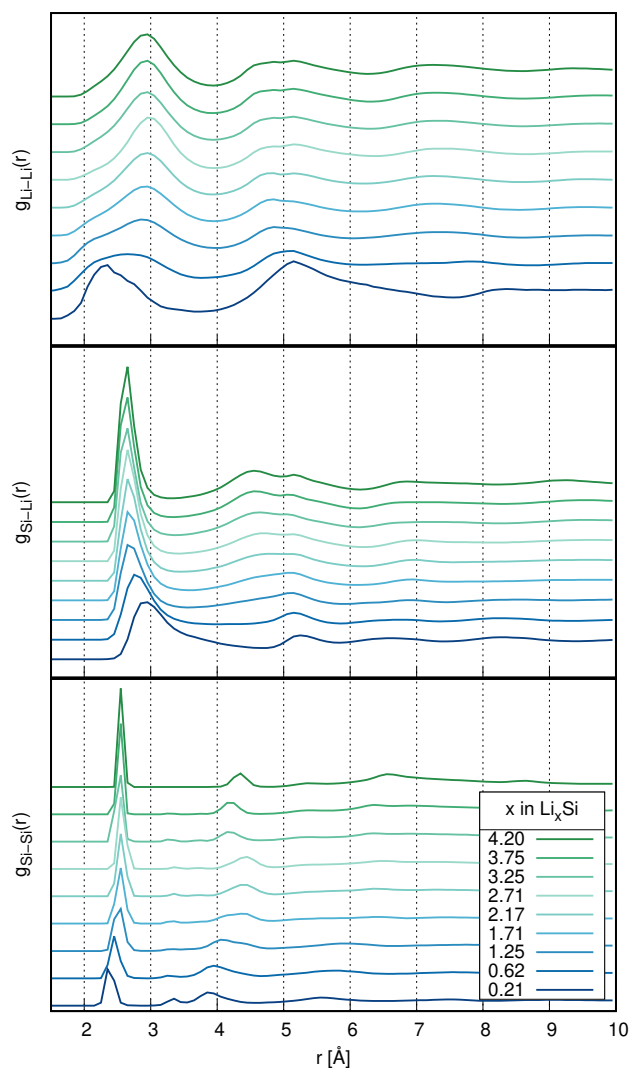


**Fig. 4** Radial pair distribution function of Li-Li, Si-Li and Si-Si for the minimized structures. Each plot shows a curve for each lithium concentration value considered in the simulations.

Si-Li coordination sphere. For $x > 1.0$ the contribution of second neighbour Li atoms interconnected with two or three Li atoms of the first Si-Li coordination sphere starts to become important and the contribution of the unconnected Li starts to decrease. For $x > 3.0$ the contribution of the first peak of the second Li neighbour atoms interconnected two or three times becomes relevant and contributions of four or more interconnections appear.

### 3.2 Coordination number

The coordination number (CN), also called ligancy, of a given atom in a chemical system, is defined as the number of atoms, molecules or ions bonded to it. To define this quantity for the present case, we have considered the number of neighbours surrounding a given atom type, using the RDF to define a cutoff distance. The average coordination number of Si atoms by other Si atoms $CN_{Si-Si}$ was calculated by counting the number Si neighbours of each Si atom, using a cutoff distance of 3.0 Å. The same
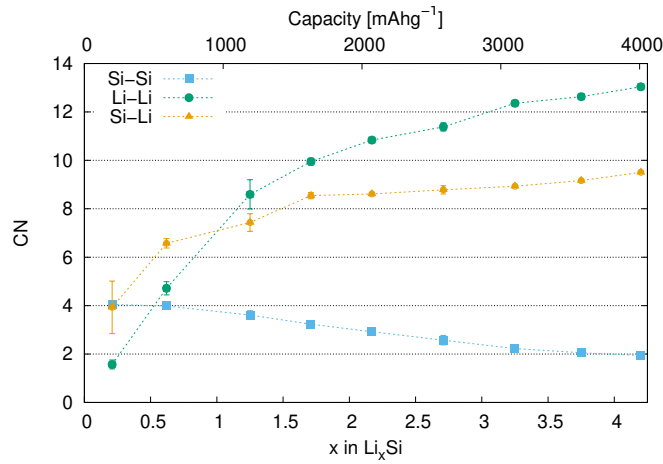
**Fig. 5** First average coordination number as function of lithium concentration for Li-Li, Si-Li and Si-Si. The distance after the first peak of the corresponding RDF was taken as the cutoff radius.



**Fig. 6** Average of the second coordination number as a function of lithium concentration for Li-Li, Si-Li and Si-Si. To choose the distances delimiting the shell on which to count the neighbours, the second peak in the corresponding RDF was considered.

was done for $CN_{Li-Li}$ with a cutoff radius equal to 4.0 Å. In the case of the $CN_{Si-Li}$ the distance corresponding to the minimum between the first and the second peaks of the RDF was considered as a cutoff radius. The results are shown in Figure 5.

In the case of $CN_{Si-Si}$, this quantity is found to decrease from 4 down to 2, as Li concentration increases. This indicates that at low $x$ the Si structure maintains the tetrahedral connection, while for large $x$ the Si atoms tend to form 1-periodic chains. Isolated Si atoms are not obtained even at the highest concentration of Li employed here, using the cutoff criterion of 3.0 Å mentioned above. For $x > 3$ the CN is close to 2. By analyzing the formation of clusters, it is found that the amorphous Si structures cannot be classified into different types of clusters, but the structures rather reflect an amorphous network (see Figure S3 in the Supporting Information). In this network of silicon, a 3-periodic structure is seen for the lower values of $x$, where the CN is around 4.0. Then a 1-periodic structure is reached for high values of $x$, where the Si-Si bonds tends to form chains, that can be seen at CN=2.05 for $x = 3.75$, for example. The Si-Li and Li-Li CN present low values for small $x$ and increase monotonically until reaching values close to 10 and 12 respectively, resembling the value of a close-packing structure.

Results for the second coordination number are presented in Figure 6. These results were obtained considering a shell with internal and external cutoff radii, chosen so as to include the second peak of the RDF. The choice of the cutoff radii varied depending on the types of atoms considered. In all cases the first CN cutoff radius was used as the second CN internal cutoff radius. The second CN external cutoff radius was 5.0 Å for Si-Si and 6.0 Å for Li-Li and Si-Li.

For the values of Si-Si second CN, an increase is observed for low Li concentrations as compared with the first CN. At large $x$, it can be found that the second CN also tends to two, something that is coherent with the formation of chains noted above. The qualitative trend for the Li-Li and Si-Li second CN is the same as that was observed for the first CN. In these cases, it starts around 5
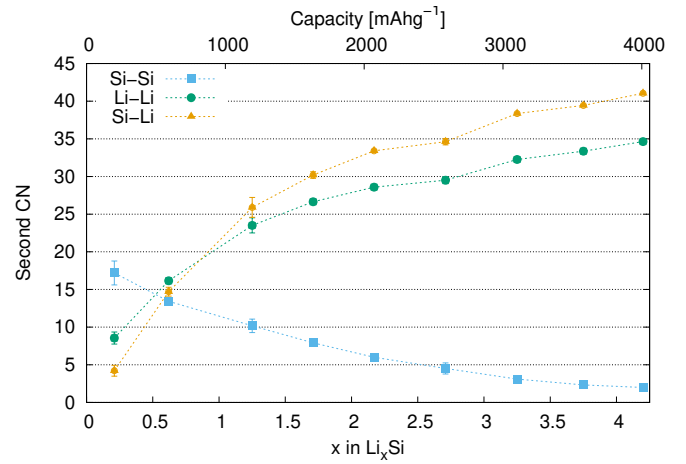
and tends to 35 and 40, respectively. This number is much higher than the one corresponding to the number of second neighbours in a close-packing structure, that is 6.0 for a face-centered cubic (FCC) structure. It is even higher than the sum of second (6) and third (24) neighbours expected for the FCC lattice.

### 3.3 Short range order

The term short-range order (SRO) is used to denote the arrangement of atoms surrounding a specific one in a shell, usually of one or two interatomic distances. Similarly, the term clustering has been defined as the tendency of similar atoms to be close to each other. Both concepts referrer to a structural order among neighbouring atoms, but not necessary persistent at longer distances. Warren[59] and Cowley[60] have defined a parameter (WCP) to characterize these types of arrangements as follows:

$$WCP = 1 - \frac{p_{A-B}}{m_B} = 1 - \frac{p_{B-A}}{m_A}, \qquad (5)$$

where $p_{A-B}$ ($p_{B-A}$) is the probability of having an atom $B$ ($A$) as a neighbour of an atom $A$ ($B$) and $m_B$ ($m_A$) is the global concentrations of atoms $B$ ($A$), expressed in molar fractions. The equality, in both possible definitions of WCP, comes from the fact that the probability of finding an atom $A$ as neighbour of and atom $B$ is equal to that of finding an atom $B$ as a neighbour of and atom $A$, that is, $m_A p_{A-B} = m_B p_{B-A}$.

The value obtained by WCP parameter in $A_xB$ systems indicates complete randomness if it is equal to zero, preference for unlike neighbours if WCP<0 and preference for similar neighbours (clustering) if WCP>0. Although this parameter enables a remarkable quantitative analysis, it is defined only for crystalline systems where each atom has the same number of neighbours[59].

We have extended this idea to define a new parameter ($\theta_{A-B}$), which is suitable for amorphous structures, as follows:

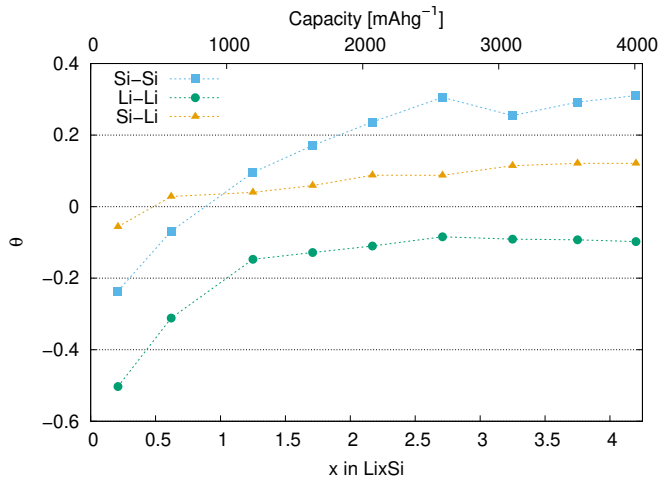$$\theta_{A-B} = \ln\left(\frac{C_{A-B}}{C_{Bulk}}\right), \qquad (6)$$

**Fig. 7** $\theta_{Li-Li}$, $\theta_{Si-Si}$ and $\theta_{Si-Li}$ parameters as a function of the Li concentration. The first subscript indicates the atom type that we are considering as central atom, and the second one, the neighbouring atom type. The cutoff radius was chosen after the first peak of the RDF.

where $A$ indicates the nature of the central atom considered and $B$ is the neighbouring atom type, equivalent to the definition of WCP. In this case the ratio between the surrounding and global concentration is calculated by the integration of the radial pair distribution function ($g_{A-B}(r)$) in a sphere around the central atom:

$$\frac{C_{A-B}}{C_{Bulk}} = \frac{1}{V(r_{cut})} \int_0^{r_{cut}} g_{A-B}(r)dV, \qquad (7)$$

where $r_{cut}$ and $V(r_{cut})$ are the cutoff radius and volume of the sphere considered. Since $g_{A-B}(r)$ has no angular dependence $dV$ can be written as $4\pi r^2 dr$. The ratio $\frac{C_{A-B}}{C_{Bulk}}$ can be thought as the average concentration inside the shell between 0 and $r_{cut}$ relative the bulk. Thus, similarly to WCP parameter, $\theta$ indicates the SRO tendency of clustering for any given atomic species. If $\theta$ is larger than zero it indicates an accumulation of atoms relative to the bulk, while if it is smaller than zero it indicates depletion. If it is equal to zero it indicates randomness. This new parameter also satisfies the relationship $\theta_{A-B} = \theta_{B-A}$ in the same way as it was discussed for WCP, since by definition $g_{A-B}(r) = g_{B-A}(r)$. So the parameter $\theta_{A-B}$ gives a similar information to that provided by the WCP , but it is applicable to amorphous systems.

Figure 7 shows the variation of the $\theta$ parameter as function of Li concentration, $x$. There are three possibilities to analyze in Li$_x$Si systems ($\theta_{Li-Li}$, $\theta_{Si-Si}$ and $\theta_{Si-Li}$) since $\theta_{Li-Si} = \theta_{Si-Li}$. In all cases, the cutoff radius was chosen after the first peak of the corresponding radial pair distribution function.

As a general trend, it can be noticed that all $\theta$s increase when $x$ increases, and that they stabilise for large $x$ values. This monotonic behaviour and the decrease in slope for high concentrations correlate with the results presented in the analysis of the coordination numbers (CN).

In the case of $\theta_{Si-Si}$, it reaches an approximately positive constant value for $x > 2.5$, showing a strong correlation with the presence of the linear Si chain, previously discussed and observed in Figure 2. Although the presence of these chains can be inferred from the CN values at the higher $x$, $\theta$ is more sensitive to SRO,

since it is normalized by the bulk concentration. This property of $\theta$ allows to make a clearer analysis even if the chains are interacting with each other, as it is the case for low Li concentrations.

$\theta_{Si-Li}$ presents a small variation and a positive value for all $x > 0.5$ showing an approximately constant accumulation of Li around Si, or analogously an accumulation of Si around Li. This behaviour may be attributed to the strong attractive interaction between Si-Li. In the case of $\theta_{Li-Li}$, this parameter is always negative, indicating a weak Li-Li interaction and the corresponding depletion of Li-Li neighbours. Finally, the parameter $\theta_{Si-Si}$ has negative values for $x < 1.0$, suggesting that the presence of a small concentration of lithium tends to drive Si apart from each other. However, $\theta_{Si-Si}$ becomes positive when $x > 1.0$, implying an accumulation of Si-Si neighbours relative to the bulk. This is due to the formation of Si-Si SRO structures. For $x > 2.5$ a constant value of $\theta_{Si-Si} \cong 0.3$ can be observed, revealing the formation of stable Si-Si SRO structures given by the Si-Si chains mentioned above.

## 4    Conclusions

Aiming to emulate the amorphous structures found in many experimental electrochemical experiments, we have generated disordered structures of Li$_x$Si alloys for several values of $x$ using an accelerated dynamic algorithm and a reactive force field. The volume change of the lithiated structures relative to the bulk Si material was in concordance with experimental AFM results. The blinded accelerated exploration of local minima (AELM) allowed to characterize a wide range of amorphous structures. The energies of the structures obtained represent well the electrochemical behavior of the potential curve in function of Li concetration. Their radial distribution function was analyzed for the different types atomic pairs and the complex structure of the second peak of the Li-Si RDF was elucidated by a cluster interconnection analysis. Also, by doing an analysis of the cluster formation as a function of the cutoff radius, we showed that the amorphous structures do not present different Si bonds or isolated Si atoms. Instead, we found that that the system behaves like an amorphous network. Studying the first and second coordination numbers for the different concentrations we showed that this amorphous network maintains the tetrahedral connections for low concentrations of Li and that it tends to form chains for high Li concentrations. Finally, the definition of a new parameter allowed us to determine the short-range order of the amorphous structures, defined by weak Li-Li interactions and strong Li-Si and Si-Si interactions. The new AELM method proposed here is found to be fast and effective to obtain energetically relevant minima. An analogy with multiple simulated annealing is made. A detailed analysis of AELM efficiency in comparison with other efficient methods like multiple annealing or MC methods is a motivation for further work.

## Conflicts of interest

There are no conflicts to declare.

## Acknowledgements

## Notes and references

1 S. Wang, B. Yang, H. Chen and E. Ruckenstein, *Journal of Materials Chemistry A*, 2018, **6**, 6815–6821.

2 S. Wang, B. Yang, H. Chen and E. Ruckenstein, *Energy Storage Materials*, 2019, **16**, 619–624.

3 H. Yang, S. Kannappan, A. S. Pandian, J.-H. Jang, Y. S. Lee and W. Lu, *Nanotechnology*, 2017, **28**, 445401.

4 D. Uxa, B. Jerliu, E. Hüger, L. Dörrer, M. Horisberger, J. Stahn and H. Schmidt, *The Journal of Physical Chemistry C*, 2019, **123**, 22027–22039.

5 M. Obrovac and L. Christensen, *Electrochemical and Solid State Letters*, 2004, **7**, A93.

6 B. Key, M. Morcrette, J.-M. Tarascon and C. P. Grey, *Journal of the American Chemical Society*, 2011, **133**, 503–512.

7 F. Fan, S. Huang, H. Yang, M. Raju, D. Datta, V. B. Shenoy, A. C. Van Duin, S. Zhang and T. Zhu, *Modelling and Simulation in Materials Science and Engineering*, 2013, **21**, 074002.

8 A. C. Van Duin, A. Strachan, S. Stewman, Q. Zhang, X. Xu and W. A. Goddard, *The Journal of Physical Chemistry A*, 2003, **107**, 3803–3811.

9 S. Chen, A. Du and C. Yan, *Computational Materials Science*, 2020, **183**, 109811.

10 K. J. Kim and Y. Qi, *The Journal of Physical Chemistry C*, 2015, **119**, 24265–24275.

11 B. Ding, H. Wu, Z. Xu, X. Li and H. Gao, *Nano Energy*, 2017, **38**, 486–493.

12 S.-P. Kim, D. Datta and V. B. Shenoy, *The Journal of Physical Chemistry C*, 2014, **118**, 17247–17253.

13 F. Fan, H. Yang and Z. Zeng, *Scripta Materialia*, 2018, **152**, 74–78.

14 L. Cao, H. Yang and F. Fan, *Physics Letters A*, 2019, **383**, 125955.

15 J. Tang, Q. Yin, Q. Wang, Q. Li, H. Wang, Z. Xu, H. Yao, J. Yang, X. Zhou, J.-K. Kim *et al.*, *Nanoscale*, 2019, **11**, 10984–10991.

16 A. Ostadhossein, E. D. Cubuk, G. A. Tritsaris, E. Kaxiras, S. Zhang and A. C. Van Duin, *Physical Chemistry Chemical Physics*, 2015, **17**, 3832–3840.

17 S. Basu, N. Koratkar and Y. Shi, *Acta Materialia*, 2019, **175**, 11–20.

18 M. Trochet and N. Mousseau, *Physical Review B*, 2017, **96**, 134118.

19 K. J. Kim, J. Wortman, S.-Y. Kim and Y. Qi, *Nano letters*, 2017, **17**, 4330–4338.

20 Y.-T. Zheng, M. He, G.-x. Cheng, Z. Zhang, F.-Z. Xuan and Z. Wang, *Chemical Physics Letters*, 2019, **732**, 136665.

21 Y.-T. Zheng, M. He, G.-x. Cheng, Z. Zhang, F.-Z. Xuan and Z. Wang, *Journal of Power Sources*, 2020, **459**, 228100.

22 O. Verners and A. Simone, *Mechanics of Materials*, 2019, **136**, 103030.

23 J. F. Dama, M. Parrinello and G. A. Voth, *Phys. Rev. Lett.*, 2014, **112**, 240602.

24 L. Sutto, S. Marsili and F. L. Gervasio, *Wiley Interdiscip. Rev. Comput. Mol. Sci.*, 2012, **2**, 771–779.

25 A. Barducci, M. Bonomi and M. Parrinello, *Wiley Interdiscip. Rev. Comput. Mol. Sci.*, 2011, **1**, 826–843.

26 A. Barducci, G. Bussi and M. Parrinello, *Physical Review Letters*, 2008, **100**, 20603.

27 C. Chipot, *Wiley Interdisciplinary Reviews: Computational Molecular Science*, 2014, **4**, 71–89.

28 C. F. Abrams and G. Bussi, *Entropy*, 2014, **16**, 163–199.

29 A. Liwo, C. Czaplewski, S. Ołdziej and H. a Scheraga, *Curr. Opin. Struct. Biol.*, 2008, **18**, 134–139.

30 A. Pohorille and C. Chipot, *Free Energy Calculations: Theory and Applications in Chemistry and Biology*, Springer, 2007, vol. 86.

31 G. Ciccotti and E. Vanden-Eijnden, *The European Physical Journal Special Topics*, 2015, **224**, 2515–2518.

32 S. A. Paz and E. P. M. Leiva, *J. Chem. Theory Comput.*, 2015, **11**, 1725–1734.

33 S. A. Paz, E. Vanden-Eijnden and C. F. Abrams, *Chemical Science*, 2017, **8**, 1225–1232.

34 S. A. Paz, L. Maragliano and C. F. Abrams, *Journal of Chemical Theory and Computation*, 2018, **14**, 2743–2750.

35 D. Perez, B. P. Uberuaga, Y. Shim, J. G. Amar and A. F. Voter, *Annu. Reports Comput. Chem. Vol. 5*, Elsevier, 2009, pp. 79–98.

36 A. F. Voter, F. Montalenti and T. C. Germann, *Annual Review of Materials Research*, 2002, **32**, 321–346.

37 K. a. Fichthorn and S. Mubin, *Comput. Mater. Sci.*, 2015, **100**, 104–110.

38 X. Zhou and Y. Jiang, *Computational Science – ICCS 2007*, 2007, **4487**, 826–833.

39 Y. Shim, J. G. Amar, B. P. Uberuaga and A. F. Voter, *Physical Review B*, 2007, **76**, 205439.

40 R. Ferrando, *Frontiers of Nanoscience*, 2016, **10**, 75–129.

41 L. Pavan, K. Rossi and F. Baletto, *Journal of Chemical Physics*, 2015, **143**, 184304.

42 L. M. Farigliano, S. A. Paz, E. P. M. Leiva and M. M. A. Villarreal, *Journal of Chemical Theory and Computation*, 2017, **13**, 3874–3880.

43 L. M. Farigliano, M. A. Villarreal, E. P. Leiva and S. A. Paz, *Journal of Physical Chemistry C*, 2020, **124**, 24009–24016.

44 S. Kirkpatrick, C. D. Gelatt and M. P. Vecchi, *SCience*, 1983.

45 G.-F. Hao, W.-F. Xu, S.-G. Yang and G.-F. Yang, *Sci Rep*, 2015, **5**, 15568.

46 A. Jain, S. P. Ong, G. Hautier, W. Chen, W. D. Richards, S. Dacek, S. Cholia, D. Gunter, D. Skinner, G. Ceder and K. A. Persson, *APL Materials*, 2013, **1**, 011002.

47  S. Nosé, *The Journal of chemical physics*, 1984, **81**, 511–519.

48  W. G. Hoover, *Physical review A,* 1985, **31**, 1695.

49  S. Plimpton, *Journal of computational physics*, 1995, **117**, 1–19.

50  S. A. Paz, *GEMS Is an Extensible Molecular Simulator*, `https://github.com/alexispaz/GEMS`, 2020.

51  G. Wypych, *Handbook of material weathering*, Elsevier, 2018.

52  A. F. Voter, *Physical Review Letters*, 1997, **78**, 3908.

53  A. F. Voter, *The Journal of chemical physics*, 1997, **106**, 4665–4677.

54  L. Beaulieu, T. Hatchard, A. Bonakdarpour, M. Fleischauer and J. Dahn, *Journal of the Electrochemical Society*, 2003, **150**, A1457.

55  V. Chevrier and J. R. Dahn, *Journal of the Electrochemical Society*, 2009, **156**, A454.

56  T. Hatchard and J. Dahn, *Journal of The Electrochemical Society*, 2004, **151**, A838.

57  P. Lamparter, *Physica Scripta*, 1995, **1995**, 45.

58  J. Ding, E. Ma, M. Asta and R. O. Ritchie, *Scientific reports*, 2015, **5**, 1–9.

59  B. E. Warren, *X-ray diffraction*, Dover publications, 1969.

60  J. Cowley, *Physical Review*, 1950, **77**, 669.